Proc. Natl. Acad. Sci. USA
Vol. 95, pp. 13453–13458, November 1998
Biochemistry

Impaired osteoclastic bone resorption leads to osteopetrosis in cathepsin-K-deficient mice

PAUL SAFTIG*†, ERNST HUNZIKER‡, OLAF WEHMEYER*, SHEILA JONES§, ALAN BOYDE§, WINFRIED ROMMERSKIRCH¶, JÖRG DETLEV MORITZ‖, PETER SCHU*, AND KURT VON FIGURA*

*Zentrum Biochemie und Molekulare Zellbiologie, Abteilung Biochemie II, Universität Göttingen, Gosslerstrasse 12 d, 37073 Göttingen, Germany; ‡Universität Bern, M.E. Müller-Institut für Biomechanik, Murtenstrasse 35, CH-3010 Bern, Switzerland; §Department of Anatomy and Developmental Biology, University College London, Gower Street, London WC1E 6BT, United Kingdom; ¶Institut für Biochemie, Universität Jena, Löbder Strasse 3, 07740 Jena, Germany; and ‖Zentrum Radiologie, Universität Göttingen, Robert-Koch-Strasse, 37073 Göttingen, Germany

Edited by Elizabeth F. Neufeld, University of California, Los Angeles, School of Medicine, Los Angeles, CA, and approved September 5, 1998 (received for review June 23, 1998)

ABSTRACT **Cathepsin K is a recently identified lysosomal cysteine proteinase. It is abundant in osteoclasts, where it is believed to play a vital role in the resorption and remodeling of bone. Pycnodysostosis is a rare inherited osteochondrodysplasia that is caused by mutations of the cathepsin-K gene, characterized by osteosclerosis, short stature, and acroosteolysis of the distal phalanges. With a view to delineating the role of cathepsin K in bone resorption, we generated mice with a targeted disruption of this proteinase. Cathepsin-K-deficient mice survive and are fertile, but display an osteopetrotic phenotype with excessive trabeculation of the bone-marrow space. Cathepsin-K-deficient osteoclasts manifested a modified ultrastructural appearance: their resorptive surface was poorly defined with a broad demineralized matrix fringe containing undigested fine collagen fibrils; their ruffled borders lacked crystal-like inclusions, and they were devoid of collagen-fibril-containing cytoplasmic vacuoles. Assaying the resorptive activity of cathepsin-K-deficient osteoclasts *in vitro* revealed this function to be severely impaired, which supports the contention that cathepsin K is of major importance in bone remodeling.**

Skeletal remodeling is a continuous process that involves both the resorption and formation of bone. At their site of attachment, osteoclasts generate an acidic microenvironment within which bone demineralization and matrix degradation occur. Active proteases released from osteoclasts into the resorption lacunae are known to be involved in matrix degradation (1), and it has been suggested that cysteine proteinases play a vital role in this process (2–4).

Cathepsin K (EC 3.4.22.38), a member of the papain—cysteine protease family, has been identified by several groups, as well as having been cloned from human, rabbit, and murine osteoclast libraries (5–11). By means of *in situ* hybridization and immunolocalization (5, 7, 8), cathepsin K has been shown to be highly and selectively expressed within human osteoclasts; the other cysteine proteinases (cathepsin B, L, or S) appear to be absent or present at very low levels (8).

Overexpressed baculovirus cathepsin K is known to degrade bone-matrix proteins, type I and type II collagen, and osteopontin and osteonectin at low pH (12, 13). The view that cathepsin K plays a major role in bone resorption is strengthened by the recent identification of cathepsin-K gene mutations, which are linked to pycnodysostosis, a hereditary bone disorder in which osteoclast function in bone resorption is defective (14). Pycnodysostosis is characterized by a variable clinical picture that includes short stature, open fontanelles, obtuse mandibular angles, partial or total aplasia of the terminal phalanges, a predisposition to bone fractures, and an increased roentgenographic density of the entire skeleton (15, 16).

To investigate the putatively crucial role of cathepsin K in bone resorption, we generated cathepsin-K-deficient mice by targeted inactivation of the cathepsin-K gene. Cathepsin-K-deficient mice develop osteopetrosis and manifest an impaired resorption of bone matrix; their osteoclasts exhibit a modified morphology. These mice may represent a valuable animal model for pycnodystostosis.

METHODS

Generation of Mice with Targeted Disruption of Cathepsin K. A 461-bp mouse cathepsin-K cDNA fragment corresponding to the amino acid Cys 117 to Trp270 (a gift from D. Brömme) was used to screen a genomic λ-EMBL-3 (Stratagene) library. A clone containing exons 6 to 8 of the mouse cathepsin-K gene was isolated. The cathepsin-K mouse gene was mapped by using the interspecific backcross DNA panel (The Jackson Laboratory; ref. 17) to the central mouse chromosome 3, cosegregating with cathepsin S. The neomycin phosphotransferase gene (*Neo*) was inserted in the *Hind*III site at the cDNA nucleotide position 857 under the control of the phosphoglycerokinase promoter (18). Insertion of the *Neo* cassette introduces a premature translational stop codon into the open reading frame of the cathepsin-K gene. The target construct, pCK-Kpn(*Neo*) (Fig. 1*a*, part II) was used to disrupt the cathepsin-K gene in embryonic stem cells, which were cultured as previously described (19). G418-resistant clones were screened by Southern analysis of genomic DNA, which was digested with *Bgl*II and probed with the 5′ probe (see Fig. 1*a*, parts I and III). Mutated embryonic stem cells were microinjected into blastocysts of C57BL/6J females. The resulting chimeras were used to generate heterozygous and subsequently homozygous mutant offspring against an outbred 129SVJ-C57BL/6J genetic background. Mice were genotyped for the introduced cathepsin-K gene mutation by analysis of genomic-tail DNA by using exon-6-specific PCR (primers CTSK-16: 5′-gccacacccacaccctagaag-3′ and CTSK-17: 5′-acaagtgtacattcccgtacc-3′).

Reverse Transcription–PCR (RT-PCR), Northern and Western Blot Analyses. RT-PCR was performed by using the primers CTSK-5′ (5′-atgtgggggctcaaggttctg-3′) and CTSK-3′ (5′-catatgggaaagcatcttcagagtc-3′) and the Pharmacia RT-PCR

The publication costs of this article were defrayed in part by page charge payment. This article must therefore be hereby marked "*advertisement*" in accordance with 18 U.S.C. §1734 solely to indicate this fact.

This paper was submitted directly (Track II) to the *Proceedings* office.
Abbreviations: RT-PCR, reverse transcription–PCR; SEM, scanning electron microscopy.
†To whom reprint requests should be addressed. e-mail: saftig@uni-bc2.gwdg.de.

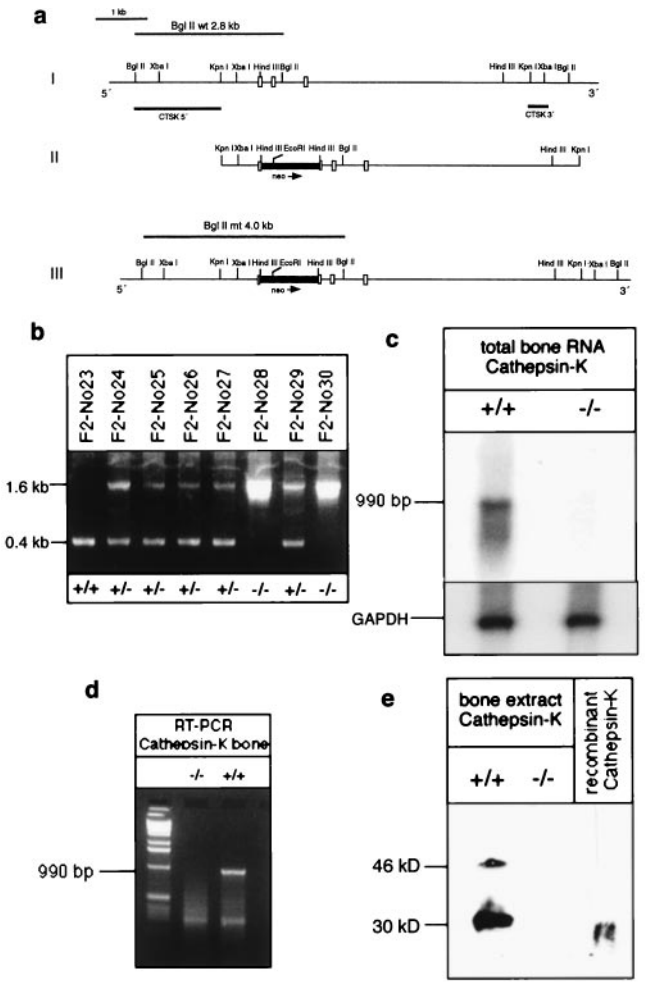

FIG. 1. Targeted disruption of the cathepsin-K gene. (*a*) Strategy for inactivation of the cathepsin-K gene by homologous recombination in embryonic stem cells. (Part I) 10-kbp portion of the cathepsin-K gene, depicting salient structural information. Exons are indicated by open boxes, flanking introns by solid vertical lines. Horizontal bars, designated as cathepsin-K probes 3′ and 5′, denote the DNA probes used for Southern blot analyses. (Part II) Targeting vector pCK-Kpn(*neo*) with 5.3-kbp homology to the cathepsin-K gene locus. The *neo*-cassette was inserted into a *Hin*dIII restriction site in exon 7. Arrowhead indicates the direction of transcription of the *neo* gene. (Part III) Predicted *ctsk* gene locus after homologous recombination. (*b*) PCR analysis of tail-genomic DNA with an exon-specific PCR amplifying a 0.4-kb fragment in wild-type (+/+) mice, 0.4-kb and 1.6-kb fragment in heterozygous (+/−) mutants, and a 1.6-kb fragment in homozygous (−/−) cathepsin-K-deficient animals. (*c*) Northern blot analysis of cathepsin-K expression. Total RNA (10 μg) was hybridized by using murine cathepsin-K and glyceraldehyde-3-phosphate dehydrogenase cDNA probes. (*d*) RT-PCR of total bone RNA and cathepsin-K-specific primers. In +/+ mice, a 990-bp fragment is amplified, whereas in −/− mice there is no amplification. (*e*) Western blot analysis of cathepsin-K expression by using an antiserum against mouse cathepsin K (37). In +/+ bone extracts, the 46-kDa cathepsin-K precursor and the 30-kDa mature form are revealed. In −/− bones, no cathepsin-K gene product is apparent. Recombinant mouse cathepsin K served as a control.

system. Total RNA from the long bones of 4-week-old mice was prepared as described by Chirgwin *et al.* (20). RNA (10 μg) was separated on a formaldehyde agarose gel and processed as described previously (21). Filters were hybridized subsequently with the murine cathepsin-K cDNA probe and then with glyceraldehyde-3-phosphate dehydrogenase.

For the Western blot analysis, bone cells derived from the long bones of six 4-day-old mice were collected, solubilized in Laemmli-buffer, separated by SDS/PAGE and transferred to a poly(vinylidene difluoride) membrane. Cathepsin-K-specific rabbit antibodies were obtained from T. Kamiya, Y. Kobayashi, and H. Sakai (Nagasaki University, Japan); they were used at a dilution of 1:1000 (22). Analysis was performed by using an enhanced chemiluminescence light-based immunodetection system (Amersham).

Radiographs. Wet unfixed long bones and vertebrae were freed from soft tissues before radiography (high-resolution soft x-ray system, DIMA Soft P41, Feinfocus, Garbsen, Germany). The same radiation energy (30 kV) and exposure times were used for the skeletal elements of both cathepsin-K-deficient and control mice. Pictures were stored as digital files and processed by using the FCR 9000 HQ system (Fuji).

Determination of the Rate of Longitudinal Bone Growth. Two 4-week-old mice of each genotype were injected intraperitoneally with the fluorochrome calcein (10 mg per kg of body weight) (Fluka) 4 days before sacrifice. The tibiae of calcein-injected animals were fixed in 2.5% formaldehyde, dehydrated in ethanol and embedded in methyl methacrylate. Ten-micrometer-thick frontal sections were cut and examined in a Leitz incident-light fluorescence microscope. Distances between the zone of vascular invasion within the growth plate and the proximal end point of the calcein label in the metaphysis were determined by using an eye-piece micrometer. Growth measurements were made at five different positions, selected by a systematic sampling process. The height of the growth plate was determined and the daily growth rate calculated from growth during a 4-day period (23).

Standard Histology. Bones were fixed in 2.5% formaldehyde in 0.1 M sodium cacodylate buffer (pH 7.4) and 0.5% $CaCl_2$ for 2 days at ambient temperature, dehydrated and embedded in methyl methacrylate. Sections (200 μm) were cut with a Leica Polycut E (Leica, Deerfield, IL) and surface stained with basic fuschin, McNeil's tetrachrome, and toluidine blue O (24).

Osteoclast Staining. Methyl methacrylate sections (5 μm thick) derived from four wild-type and four cathepsin-K knockout mice were stained with tartrate-resistant acid phosphatase (25). To facilitate the identification of osteoclasts (red) during quantification of their volume-density in trabecular and subperiosteal cortical bone, counterstaining with hemtoxylin was omitted. Beginning at a random starting point on the left-hand side, three areas covering approximately 80% of the metaphyseal area immediately beneath the growth plate were analyzed according to a systematic random sampling method. The subperiosteal analysis of osteoclast volume proportion along the cortical bone surface (immediately beneath the epiphyseal–metaphyseal junction) was conducted in a similar manner. The percentage of the cortical bone surface covered by osteoclasts was estimated by using intersection counting and a line grid. Osteoclast volume proportion was estimated by using point counting (26).

Electron Microscopy of Osteoclasts. Both tibiae and femura of four animals were fixed in 2.5% glutaraldehyde in 0.1 M sodium cacodylate buffer (pH 7.4) for 12 hours at ambient temperature. After being rinsed three times for 20 min in the same buffer, the material was postfixed for 6 hours in 1% osmium tetroxide (in 0.1 M sodium cacodylate buffer), dehydrated in acetone and embedded (six +/+ and four −/− blocks from different regions) in Epon 812 (Fluka). Semithin sections were cut with a Leica Ultracut S Microtom. Ultrathin sections were prepared, stained with uranyl acetate and examined in a Hitachi H600-B-electron microscope (Hitachi, Tokyo) (27). The thin sections were scanned systematically and all osteoclasts encountered were photographed. Sixty osteoclasts of each genotype derived from different bone regions were studied.

Scanning Electron Microscopy (SEM). Long bones, longitudinally sectioned with a razor blade, were prepared for 3-D

morphological imaging in the scanning electron microscope by cleaning in hydrogen peroxide or sodium hypochlorite. They were then dehydrated in ethanol, air dried and carbon coated by evaporation. In regions where the marrow cavity had been inadequately exposed, the dry peroxide- cleaned bones were opened by using a plain tungsten carbide bur in a dental handpiece. The samples were imaged in a Zeiss DSM962 digital scanning electron microscope operated at 20 or 30 kV in the backscattered electron mode by using a KE (Toft, Cambs, UK) solid-state backscattered electron-microscopy detector (28).

Osteoclast Resorption Assay. To estimate the activity of isolated osteoclasts *in vitro*, the volume, perimeter, and area of resorptive pits were measured by confocal laser reflection microscopy (29). Long bones were removed from freshly killed 2-day-old mice, and the washed paired shafts were diced in Eagle's minimum essential medium containing 10% fetal calf serum and 2 mM L-glutamine. The bone cells were released by gentle pipetting and aliquots of the suspension were seeded onto $10 \times 10 \times 0.2$ mm slices of sperm whale dentine. After a settling time of 1 hour, the nonadherent cells were washed off and fresh medium was added for further culturing at 37°C in an atmosphere containing 5% CO_2 for 24 hours. The slices were then cleaned of free cells, rinsed with water and stained with 1% toluidine blue. The specimens were dried and resorption-pit measurements carried out as described previously (29) by using a video-rate line-confocal reflection light microscope ILM2W (Lasertech, Japan). To exclude bias, dentine specimens were coded randomly before being counted and measured. A ×40 0.95 numerical aperture dry objective, with a coverslip cemented to the objective, was used. The area and volume of pits below the surface were given by dedicated software (SIS, Münster, Germany); the mean depth of each pit was calculated from the volume:area ratio. Nonparametric data analysis was carried out by using MINITAB statistical software. To determine the thickness of demineralized organic matrix dried in the pits, dentine slices were carbon-coated and examined by SEM by using backscattered electron imaging at 10 kV and 15 kV (and secondary electron imaging for morphology at 1.25 kV).

RESULTS

Generation of Cathepsin-K-Deficient Mice. A gene-targeting vector was constructed to disrupt cathepsin K (Fig. 1*a*, parts I–III) and a homologous recombined embryonic stem cell clone (ECK-72) was used to generate chimeras that transmitted the introduced mutation to their offspring (Fig. 1*b*). Northern blotting (Fig. 1*c*), RT-PCR (Fig. 1*d*), and Western blotting (Fig. 1*e*) demonstrated a complete absence of cathepsin-K RNA and protein in homozygous cathepsin-K-deficient mice.

Heterozygotes exhibit a normal phenotype and fertility (data not shown). Genotyping of 102 offspring from heterozygote crosses (Fig. 1*b*) revealed frequencies of 25.5% for homozygous and 49.5% for heterozygous mutant mice, which are in accordance with the expected Mendelian values. Homozygous cathepsin-K-deficient mice survive and are fertile; they manifest no overt phenotypic abnormalities until the age of 10 months. The suppressed growth seen in pycnodysostosis patients (15, 16) was not observed in cathepsin-K-deficient mice.

Osteopetrosis in Cathepsin-K-Deficient Mice. Regular radiological examination of cathepsin-K-deficient mice revealed signs of osteosclerosis. Examination of skeletal preparations derived from 1-week-old mice by radiography and after alizarin staining revealed the development of the membranous bones within the skull, auditory ossicles, and clavicles to be normal (data not shown), indicating that cathepsin K deficiency affects primarily endochondral ossification. In contrast to pycnodysostotic patients, acroosteolysis of the distal phalanges, bone fragility, and clavicular dysplasia were not observed in cathepsin-K-deficient mice until the age of 10 months (data not shown).

An unusually dense trabeculation of the bone-marrow spaces was revealed on detailed radiological analyses of the long bones and vertebrae (Fig. 2*a*) of cathepsin-K knockout mice of different ages. The increased trabecular bone density was asymmetric and most pronounced in regions of rapid longitudinal growth, for example, in the distal femur and the proximal tibia. This radiological feature is typical for osteopetrosis (1, 30). The hematocrit and hemoglobin levels were normal, indicating that hematopoiesis was not compromised in cathepsin-K-deficient mice (data not shown). An osteopetrotic phenotype, characterized by the retention of cancellous bone

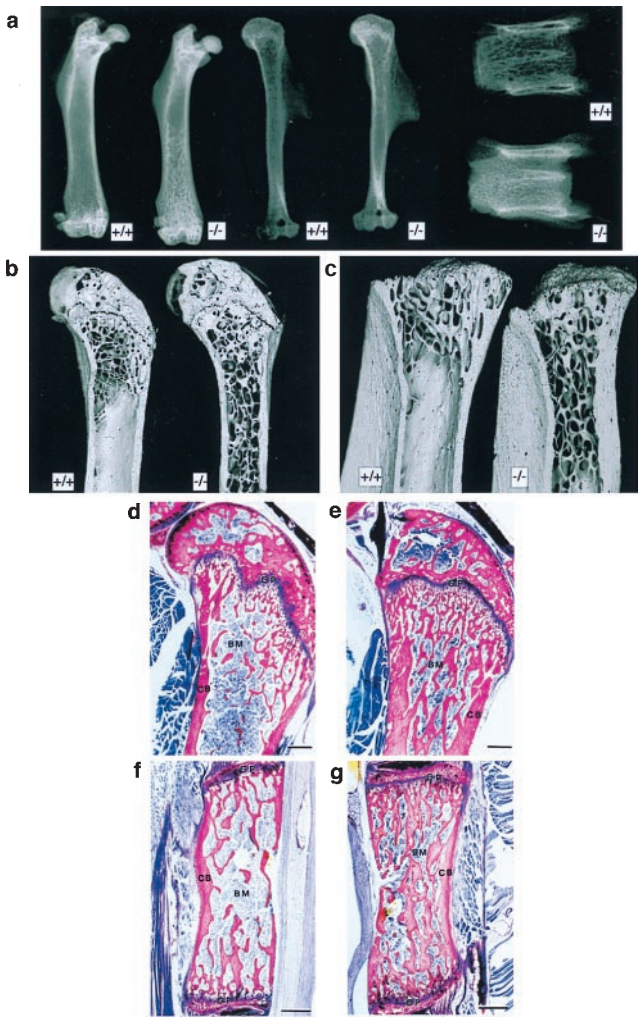

FIG. 2. Osteopetrosis in cathepsin-K deficient mice. (*a*) Radiographs of 16-week-old bones in cathepsin-K knockout (−/−) and control (+/+) mice. *Left,* femura. *Center,* humeri. Note extensive trabeculation of bone-marrow space (beginning at the distal end) in cathepsin-K-deficient mouse. *Right,* lumbar vertebrae (note the very dense and irregular distribution of spongiosa in the cathepsin-K-deficient mouse. (*b* and *c*) SEM images of 3-month-old proximal femura (*b*, with retained epiphyses) and tibiae (*c*, with epiphyses removed). Note the retention of cancellous bone in the shafts of cathepsin-K-deficient (−/−) bones. Field widths: $b = 7.69$ mm; $c = 5.84$ mm (*d* and *e*). Histological sections of the meta- and epiphysis of control (*d*) and cathepsin-K-deficient (*e*) femura embedded in methyl methacrylate and stained with McNeil's tetrachrome. Note the unresorbed primary spongiosa in *e*. (*f* and *g*) Histological sections (sagittal plane) through the ventral half of thoracic vertebrae derived from control (*f*) and cathepsin-K-deficient (*g*) mice. BM, bone marrow; CB, cortical bone; GP, growth plate. [Bars = 400 μm (*d–g*).]

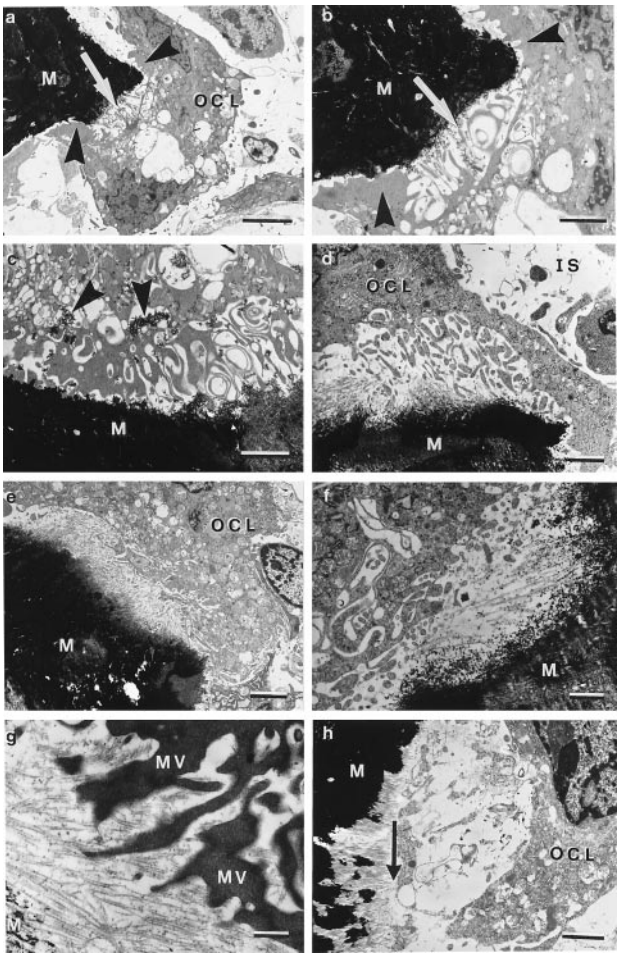

FIG. 3. Ultrastructural changes in cathepsin-K-deficient tibial osteoclasts. (*a* and *b*) Control osteoclasts (OCL). At the resorption site (arrows), these cells protrude long microplicae comprising the characteristic ruffled border. The so-called "clear" zones are indicated by arrowheads. (*c*) Ruffled border of a control osteoclast depicting electron-dense inclusions (arrowheads). (*d*) Ruffled border of a cathepsin-K-deficient osteoblast, composed of numerous slender microplicae. Note the poorly defined resorption front. IS, interstitial tissue space; M, mineralized bone matrix. (*e*) Resorption interface between a cathepsin-K-deficient osteoclast and the mineralized bone matrix (M). Numerous fine collagen fibrils have been exposed by mineral removal by the osteoclast. (*f* and *g*) Resorption pits associated with cathepsin-K-deficient osteoclasts illustrating (at higher magnifications) the collagen fibrils that persist after digestion of the mineral substance (M). MV [in (*g*)], microvilli of osteoclast. (*h*) Well orientated and clearly exposed collagen fibrils in resorption pit associated with cathepsin-K-deficient osteoclast that are digested away at a straight resorption front (arrow). [Bars = 5 μm (*a*), 2 μm (*b, c, d, h*), 3 μm (*e*), 1 mm (*f*), and 0.5 μm (*g*).]

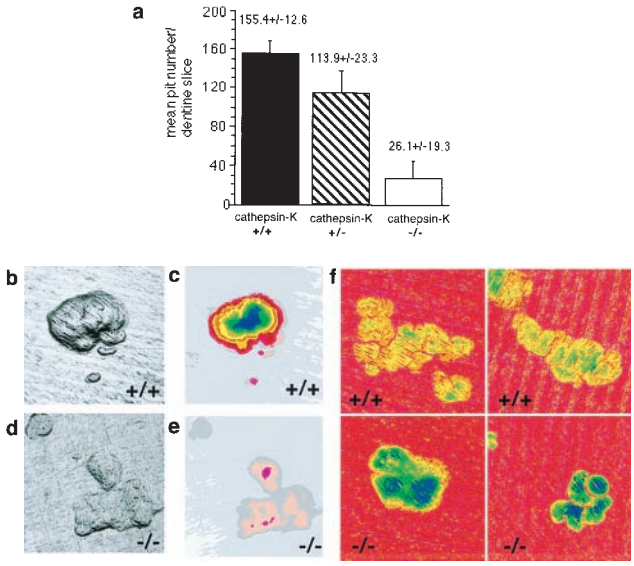

FIG. 4. Cathepsin-K-deficient osteoclasts with impaired bone resorption. Fresh osteoclasts were isolated and seeded as a suspension onto dentine sections, and (*a*) the total number of resorption pits therein was then determined. Cathepsin-K-deficient (−/−) osteoclasts formed significantly fewer resorption pits than did control (+/+) or heterozygote (+/−) ones. (Two-sample *t* test for +/+ vs. −/−: $P = 0.0001$; for ± vs. −/−: $P = 0.001$). (*b* and *d*) Images of resorption pits produced in the confocal reflection light microscope (maximum brightness; ref. 29). On dentine slices seeded with control osteoclasts (*b*), the pits are deeper and more sharply defined than on those seeded with cathepsin-K-deficient (−/−) osteoclasts (*d*). (*c* and *e*) Topographic-map images of resorption pits. Each band of color (pink, superficial; blue, deep) represents 1 μm in the vertical direction. The control pit (*c*), with characteristically steep sides, has a maximum depth of approximately 13 μm, whereas one of similar area created by a cathepsin-K-deficient osteoclast (*e*) is only about 3 μm deep. Field widths of *b–e* are 143 μm (*f*) Resorption pits analyzed by 15-kV digital backscattered electron imaging, pseudocolor coded to scale the amount of residual matrix. In cathepsin-K −/− pits, a greater thickness (more colors) of unprocessed residual matrix was found. Field width of each part = 128 μm.

in the shafts of long bones, was also demonstrated in cathepsin-K-deficient mice by means of SEM. At equivalent sites, the trabeculae in cathepsin-K-deficient mice were thicker than those in controls; plates of bone were also more common than in wild-type animals in which thinner rods were the norm (Fig. 2 *b* and *c*). In general, and in contrast to the findings concerning trabecular microarchitecture shown in Fig. 2 *b* and *c*, the external form of the cathepsin-K-deficient bones was more gracile than that of the control ones.

Histological examination of long bones and vertebrae confirmed the x-ray and SEM findings. The marrow cavities of all endochondral bones derived from cathepsin-K-deficient mice contained abundant unresorbed primary spongiosa, which reduced the effective space by up to ≈60% in the metaphyses of 5-week-old animals (Fig. 2 *d* and *e*). Primary trabeculae (i.e., those containing remnants of cartilage tissue) persisted within the epi-, meta-, and diaphyses of all long bones. The diaphyseal

Table 1. Resorption of dentine by mouse osteoclasts *in vitro*

Cathepsin-K genotype	No. of pits	Pit areas, μm^2	Pit volume, μm^3	Pit perimeter, μm	Mean depth, μm
+/+	692	573 ± 36	1,396 ± 118	101.9 ± 3.6	1.70 ± 0.041
+/−	499	590 ± 41	1,455 ± 144	102.5 ± 4.1	1.61 ± 0.043
−/−	376	706 ± 53	872 ± 65	132.9 ± 5.9	0.96 ± 0.020

Cathepsin-K-deficient osteoclasts generate pits with larger areas ($P = 0.016$) and perimeters ($P < 0.0001$), but with smaller volumes ($P = 0.077$) and depths ($P < 0.0001$) than control ones. Values represent means ± standard errors. Probabilities were determined by the nonparametric rank-order Mann–Whitney Test, adjusted for ties. (Please note: As the pits are significantly shallower in the knockout mice, there would be a bias towards detecting those with larger areas in this group, very shallow etchings being detectable only by using backscattered electron imaging.) The use of the ratio volume/area (mean depth) compensates for any such measurement bias.

cortical bone was less readily distinguished from the subjacent trabecular bone. The vertebrae of cathepsin-K-deficient mice also contained a higher than normal proportion of primary spongiosa (Fig. 2 *f* and *g*). The overall structure of epiphyseal and vertebral growth plates appeared to be normal. Although the heights of tibial growth plates were greater in cathepsin-K-deficient mice (169 μm ± 8 μm) than in controls (141 μm ± 5 μm), the daily longitudinal bone growth rates did not differ significantly between the two types of animals (not shown). The numbers of TRAP-stained osteoclasts within the tibial metaphysis (volume density in +/+, volume per total volume: 0.061 ± 0.011%; −/−, volume per total volume: 0.053 ± 0.012%), and cortex (surface density in +/+: 0.439 ± 0.14%; −/− 0.518 ± 0.16%) of cathepsin-K-deficient mice appeared not to be significantly different from controls.

Cathepsin-K-Deficient Osteoclasts Display an Altered Ultrastructural Appearance. Pycnodysostotic osteoclasts have been reported to contain large cytoplasmic vacuoles filled with bone-derived collagen fibrils and electron-dense material, presumably of mineral origin. The area of demineralized bone matrix underlying the ruffled borders of such osteoclasts was also observed to be greater than normal (31). The resorptive surface associated with normal osteoclasts in this study was sharply demarcated from the adjacent bone, and electron-dense particles were regularly observed within lacunae (Fig. 3 *a–c*). In contrast, the resorptive surface of bone in cathepsin-K-deficient osteoclasts was poorly defined, the fringe of demineralized matrix was broader (Fig. 3*d*), and lacunae were devoid of electron-dense particles (Fig. 3*d*). Compared with the wild type, the ruffled borders of these cathepsin-K-deficient osteoclasts were more irregular in conformation and extent: both very long and very short processes coexisted, and bleb-like or even circular protrusions of the plasmalemmal folds were observed (Fig. 3*f*). In wild-type osteoclasts, ruffled borders were generally well organized, the plicae being uniform in both shape and length (Fig. 3*c*). In cathepsin-K-deficient mice, a large number of very fine collagen fibrils were present within the resorption lacunae, suggesting that they persist for longer periods of time before removal (Fig. 3*g*). The collagen fibrils had been digested away at a straighter resorption front (Fig. 3*h*). Osteoclast adhesion sites in the sealing ("clear") zone of controls were generally broad and in intimate contact with the underlying bone matrix, whereas in cathepsin-K-deficient mice, these were often open and detached (not shown). As in pycnodysostotic patients (31), large irregularly shaped vacuoles were frequently found in the cytoplasm of cathepsin-K-deficient osteoclasts. However, the vacuoles lacked striated collagen fibrils as well as electron-dense crystalline material (not shown). In controls, vacuoles were of a more uniform shape and diameter; they did not contain residues of collagen fibrils, but often had electron-dense (crystalline) inclusions (not shown).

Severely Impaired Bone Resorption in Cathepsin-K-Deficient Mice. The radiological and morphological findings point to an impaired bone resorption in cathepsin-K-deficient mice. To measure their resorptive activity, osteoclasts were isolated from the shafts of the long bones of 2-day-old mice and seeded as a suspension onto dentine sections. The resorption pits were analyzed by 3-D confocal reflection mapping and conventional reflected light microscopy (29). The mean area and perimeter of pits in cathepsin-K-deficient mice were greater than in heterozygotes and controls. However, the mean volume and depth of pits were significantly reduced in cathepsin-K-deficient osteoclasts (Table 1), and their number was about 6-fold lower (Fig. 4*a*). One explanation for the changes in the size and shape of the pits made by the cathepsin-K-deficient osteoclasts is that they enter a resting state when collagen degradation is impaired (32). That osteoclastic activity was impaired was clearly revealed by confocal light microscopy (Fig. 4 *b–e*). The pits of cathepsin-K-deficient osteoclasts generally appeared very shallow and were of irregular form (Fig. 4 *d* and *e*), whereas those in controls and heterozygotes were deeper and had a more clearly defined shape (Fig. 4 *b* and *c*). The layer of demineralized organic matrix dried in the osteoclastic resorption pit reduces electron backscattering. To compare the thickness of demineralized organic matrix, cathepsin-K +/+ and −/− slices were carbon coated and examined by SEM by using backscattered electron imaging. The images were pseudocolor coded to scale the amount of residual matrix; −/− pits generally showed a greater number of colors, indicating a greater thickness of unprocessed residual matrix (Fig. 4*f*).

DISCUSSION

Most of the ultrastructural, histological, and radiological abnormalities observed in cathepsin-K-deficient mice closely resemble those described for pycnodysostotic humans. They can be accounted for by an impaired resorption of the bone matrix because of the absence of cathepsin K.

The altered ultrastructural appearance of osteoclasts in cathepsin-K-deficient mice was most likely attributable to the lack of proteolytic activity. This lack led to the formation of a relatively broad demineralized bone-matrix fringe along the resorption front (Fig. 3 *d–f*). The resorption of collagen fibrils must have been depressed, because, after mineral removal, these entities persisted longer than in controls. Osteoclastic migration tracks are easily seen in SEM preparations (28) and were found in the −/− bones (not shown). Thus cathepsin-K-deficient osteoclasts do move over the surface of the bone, which they partly resorb, and inhibition of osteoclastic movement is not responsible for the impaired resorption. Although resorption was defective in cathepsin-K-deficient mice, it was not completely inhibited. The osteoclasts appear to work inefficiently, but may partly compensate for this by protracting the resorption time. However, numbers of cells per unit tissue volume were not increased by enhanced cell-recruitment activity.

An understanding of the molecular processes underlying osteopetrosis in cathepsin-K-deficient mice might facilitate the evaluation of cathepsin-K inhibitors for therapeutic use. Such inhibitors (33) could be useful in preventing the excessive bone loss incurred in diseases such as rheumatoid arthritis and osteoporosis.

Osteopetrotic phenotypes have been observed in several spontaneous mouse mutants (op/op mouse, mi-mouse; refs. 34, 35) and in mice with experimental gene disruptions (e.g., c-fos, c-src; refs. 36, 37). The previously described mouse mutants have highlighted the importance of osteoclast differentiation from their myeloid precursors (e.g., op/op, c-fos$^{-/-}$; refs. 34, 36) and of their resorptive activity (e.g., c-src $^{-/-}$; ref. 37). As a model for osteopetrosis, the cathepsin-K-deficient mouse will furnish us with further means of probing the molecular mechanisms underlying bone resorption in both health and disease.

We thank N. Hartelt, E. Kapfinger, and M. Arora for their excellent technical assistance. We are also indebted to Drs. T. Kamiya, Y. Kobayashi, and H. Sakai (Nagasaki University, Japan) for their gift of anti-cathepsin-K rabbit antibodies and to Dr. D. Brömme for that of the cathepsin-K-specific probe and purified cathepsin K. This work was supported by the Deutsche Forschungsgemeinschaft, the Swiss National Science Foundation, and the Medical Research Council.

1. Erlebacher, A., Filvaroff, E. H., Gitelman, S. E. & Derynck, R. (1995) *Cell* **80,** 371–378.
2. Delaisse, J. M., Eeckout, Y. & Vaes, G. (1984) *Biochem. Biophys. Res. Commun.* **125,** 441–447.
3. Everts, V., Delaisse, J. M., Korper, W., Niehof, A., Vaes, G. & Beertsen, W. (1992) *J. Cell. Physiol.* **150,** 221–231.

4. Hill, P. A., Buttle, D. J., Jones, S. J., Boyde, A., Murata, M., Reynolds, J. J. & Meikle, M. C. (1994) *J. Cell Biochem.* **56,** 118–130.
5. Tezuka, K., Tezuka, Y., Maejima, A., Sato, T., Nemoto, K., Kamioka, H., Hakeda, Y. & Kumegawa, M. (1994) *J. Biol. Chem.* **269,** 1106–1109.
6. Inaoka, T., Bilbe, G., Ishibashi, O., Tezuka, K., Kumegawa, M. & Kokubo, T. (1995) *Biochem. Biophys. Res. Commun.* **206,** 89–96.
7. Li, Y. P., Alexander, M., Wucherpfennig, A. L., Yelick, P., Chen, W. & Stashenko, P. J. (1995) *J. Bone Miner. Res.* **10,** 1197–1202.
8. Drake, F. H., Dodds, R. A., James, I. E., Connor, J. R., Debouck, C., Richardson, S., Lee-Rykaczewski, E., Coleman, L., Rieman, D., Barthlow, *et al.* (1996) *J. Biol. Chem.* **271**, 12511–12516.
9. Brömme, D. & Okamoto, K. (1995) *Biol. Chem. Hoppe-Seyler* **376**, 379–384.
10. Shi, G. P., Chapman, H. A., Bhairi, S. M., DeLeeuw, C., Reddy, V. Y. & Weiss, S. J. (1995) *FEBS Lett.* **357,** 129–134.
11. Velasco, G., Ferrando, A. A., Puente, X. S., Sanchez, L. M. & Lopez-Otin, C. J. (1994) *J. Biol. Chem.* **269,** 27136–27142.
12. Bossard, M. J., Tomaszek, T. A., Thompson, S. K., Amegadzie, B. Y., Hanning, C. R., Jones, C., Kurdyla, J. T., McNulty, D. E., Drake, F. H., Gowen, M., *et al.* (1996) *J. Biol. Chem.* **271,** 12517–12524.
13. Kafienah, W., Brömme, D., Buttle, D. J., Croucher, L. J. & Hollander, A. J. (1998) *Biochem. J.* **331,** 727–732.
14. Gelb, B. D., Shi, G. P., Chapman, H. A. & Desnick, R. J. (1996) *Science* **273,** 1236–1238.
15. Maroteaux, P. & Lamy, M. (1962) *Presse Med.* **70,** 999.
16. Edelson, J. G., Obad, S., Geiger, R., On, A. & Artul, H. J. (1992) *Clin. Orthop. Relat. Res.* **280,** 264–276.
17. Rowe, L. B., Nadeau, J. H., Turner, R., Frankel, W. N., Letts, V. A., Eppig, J. T., Ko, M. S., Thurston, S. J. & Birkenmeier, E. H. (1994) *Mamm. Genome* **5,** 253–274.
18. Thomas, K. R. & Capecchi, M. R. (1987) *Cell* **51,** 503–512.
19. Köster, A., Saftig, P., Matzner, U., von Figura, K., Peters, C. & Pohlmann, R. (1993) *EMBO J.* **12,** 5219–5223.
20. Chirgwin, J. M., Przybyla, A. E., MacDonald, R. J. & Rutter, W. J. (1979) *Biochemistry* **18,** 5294–5299.
21. Isbrandt, D., Arlt, G., Brooks, D. A., Hopwood, J. J., von Figura, K. & Peters, C. (1994) *Am. J. Hum. Genet.* **54,** 454–463.
22. Kamiya, T., Kobayashi, Y., Kanaoka, K., Nakashima, T., Kato, Y., Mizuno, A. & Sakai, H. (1998) *J. Biochem.* **123,** 752–759.
23. Hunziker, E. B., Schenk, R. K. & Cruz Orive, L. M. (1987) *J. Bone Jt. Surg. Am. Vol.* **69.2,** 162–173.
24. Schenk, A. J., Olah, J. & Herrmann, W. (1984) in *Methods of Calcified Tissue Preparation*, ed. Dickson, G. R., (Elsevier Science, Amsterdam), 1–56.
25. Lindunger, A., MacKay, C. A., Ek-Rylander, B., Andersson, G. & Marks, S. C. (1990) *Bone Miner.* **10.2,** 109–119.
26. Cruz Orive, L. M. & Hunziker, E. B. (1986) *J. Microsc. (Oxford)* **143,** 47–80.
27. Hunziker, E. B., Ludi, A. & Herrmann, W. (1992) *J. Histochem. Cytochem.* **40,** 909–917.
28. Boyde, A. & Jones, S. J. (1996) *Microsc. Res. Tech.* **33,** 92–120.
29. Boyde, A. & Jones, S. A. (1995) in *Handbook of Biological Confocal Microscopy*, ed. Pawley, J. B. (Plenum, New York), pp. 255–266, 2nd Ed.
30. Felix, R., Hofstetter, W. & Cecchini, M. G. (1996) *Eur. J. Endocrinol.* **134,** 143–156.
31. (18) Everts, V., Aronson, D. C. & Beertsen, W. (1985) *Calcif. Tissue Int.* **37,** 25–31.
32. Inui, T., Ishibashi, O., Inaoka, T., Origane, Y., Kumegawa, M., Kokubo, T. & Yamamura, T. (1997) *J. Biol. Chem.* **272,** 8109–8112.
33. Thompson, S. K., Halbert, S. M., Bossard, M. J., Tomaszek, T. A., Levy, M. A., Zhao, B., Smith, W. W., Abdel-Meguid, S. S., Janson, C. A., D'Alessio, K. J., *et al.* (1997) *Proc. Natl. Acad. Sci. USA* **94,** 14249–14254.
34. Yoshida, H., Hayashi, S., Kunisada, T., Ogawa, M., Nishikawa, S., Okamura, H., Sudo, T., Shultz, L. D. & Nishikawa, S. (1990) *Nature (London)* **345,** 442–444.
35. Hodgkinson, C. A., Moore, K. J., Nakayama, A., Steingrimsson, E., Copeland, N. G., Jenkins, N. A. & Arnheiter, H. (1993) *Cell* **74,** 395–404.
36. Wang, Z. Q., Ovitt, C., Grigoriadis, A. E., Mohle-Steinlein, U., Rüther, U. & Wagner, E. F. (1992) *Nature (London)* **360,** 741–745.
37. Lowe, C., Yoneda, T., Boyce, B. F., Chen, H., Mundy, G. R. & Soriano, P. (1993) *Proc. Natl. Acad. Sci. USA* **90,** 4485–4489.